A large area diamond-based beam tagging hodoscope for ion therapy monitoring

M.L. Gallin-Martel, L. Abbassi, A. Bes, G. Bosson, J. Collot, T. Crozes, S. Curtoni, W. de Nolf, D. Dauvergne, M. Fontana, et al.

A large area diamond-based beam tagging hodoscope for ion therapy monitoring

M.-L. Gallin-Martel, L. Abbassi, A. Bes, G. Bosson, J. Collot, T. Crozes, S. Curtoni, D. Dauvergne, W. De Nolf, M. Fontana, L. Gallin-Martel, J.-Y. Hostachy, J. Krimmer, A. Lacoste, S. Marcatili, J. Morse, J.-F. Motte, J.-F. Muraz, F. E. Rarbi, O. Rossetto, M. Salomé, É. Testa, R. Vuiart, M. Yamouni

Abstract—. **The MoniDiam project is part of the French national collaboration CLaRyS (Contrôle en Ligne de l'hAdronthérapie par RaYonnements Secondaires) for on-line monitoring of hadron therapy. It relies on the imaging of nuclear reaction products that is related to the ion range. The goal here is to provide large area beam detectors with a high detection efficiency for carbon or proton beams giving time and position measurement at 100 MHz count rates (beam tagging hodoscope). High radiation hardness and intrinsic electronic properties make diamonds reliable and very fast detectors with a good signal to noise ratio. Commercial Chemical Vapor Deposited (CVD) poly-crystalline, heteroepitaxial and monocrystalline diamonds were studied. Their applicability as a particle detector was investigated using α and β radioactive sources, 95 MeV/u carbon ion beams at GANIL and 8.5 keV X-ray photon bunches from ESRF. This facility offers the unique capability of providing a focused (~1 µm) beam in bunches of 100 ps duration, with an almost uniform energy deposition in the irradiated detector volume, therefore mimicking the interaction of single ions. A signal rise time resolution ranging from 20 to 90 ps rms and an energy resolution of 7 to 9% were measured using diamonds with aluminum disk shaped surface metallization. This enabled us to conclude that polycrystalline CVD diamond detectors are good candidates for our beam tagging hodoscope development. Recently, double-side stripped metallized diamonds were tested using the XBIC (X Rays Beam Induced Current) set-up of the ID21 beamline at ESRF which permits us to evaluate the capability of diamond to be used as position sensitive detector. The final detector will consist in a mosaic arrangement of double-side stripped diamond sensors read out by a dedicated fast-integrated electronics of several hundreds of channels.**

Index Terms— **Synthetic diamond detectors, on-line monitoring of hadron therapy, charge collection efficiency, time resolution, integrated fast read out electronics**

I. INTRODUCTION

THE treatment of tumors by a beam of carbon ions or protons is an alternative cancer therapy known as hadron therapy. Ions deposit a large fraction of the dose at the end of their path, in the Bragg peak. Compared to conventional X-ray radiotherapy, hadron therapy allows a more efficient dose delivery in the tumor, with a reduction of the dose deposited in the nearby healthy organs. The conformation of the deposited dose to the tumor volume is provided by distributing Bragg peaks in this volume, either spot by spot, or by means of passive scattering and energy degradation. However, since multiple sources of uncertainty on the ion range may cause deviations from the planned dose distribution [1], online control of the ion range is desired in order to reduce safety margins and optimize the ballistic advantage of ion therapy.

During an irradiation with ion beams, nuclear reactions occur for part of the projectiles along their path in the patient body, and photons in the range 1-10 MeV are emitted almost isotropically within much less than a picosecond after the reactions. It has been shown experimentally that the longitudinal distribution of such prompt-gamma production is highly correlated to the primary ion range [2], [3]. In the CLaRyS collaboration, two systems for prompt gamma detection are currently under development [4], [5], [6]: a
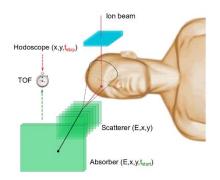

Fig. 1 Scheme of the combination of a Compton camera and a beam hodoscope for time of flight prompt-gamma range verification.

ML. Gallin-Martel, A. Bes, G. Bosson, J. Collot, S. Curtoni, D. Dauvergne, L. Gallin-Martel, JY Hostachy, A. Lacoste, S. Marcatili, JF Muraz, FE. Rarbi, O. Rossetto, R. Vuiart and M. Yamouni are with Laboratoire de Physique Subatomique et de Cosmologie, CNRS/IN2P3, Université Grenoble-Alpes, UMR 5821 38026 Grenoble Cédex France (corresponding author ML. Gallin-Martel e-mail : mlgallin@lpsc.in2p3.fr)

M. Fontana, J. Krimmer and E. Testa are with IPNL, Université de Lyon, Université Lyon 1, CNRS/IN2P3, UMR 5822, France,

W. De Nolf, J. Morse and M. Salomé are with ESRF, Grenoble, France.

L. Abbassi, T. Crozes and JF. Motte are with the Neel Institute, Université Grenoble-Alpes and CNRS UPR2940, Grenoble, France.

collimated gamma camera and a Compton camera (Fig. 1). The originality of the two systems is the use of Time Of Flight (TOF) in order to reduce the background. Depending on the beam time-structure and intensity, a beam tagging hodoscope may be necessary to detect the arrival time of ion bunches or even individual projectiles. This hodoscope will be also used for transverse position measurement, giving access to 3D prompt-gamma imaging. Thus the hodoscope plays a major role in all the detection concepts, and has to overcome the issue of providing position and timing information of the incident hadron beam at about 100 MHz count rates. The collaboration developed a scintillating-fiber based hodoscope, read-out by photomultipliers [6], [7]. In order to improve the timing resolution, and to overcome limitations such as limited count rates of photomultipliers, the collaboration initiated the MoniDiam project which aims to develop a diamond-based hodoscope and its dedicated integrated fast read-out electronics.

II. Material and methods

A. Diamond Sensors

Chemical Vapor Deposition (CVD) synthetic diamonds are grown by the technique of microwave plasma enhanced CVD. Their qualities and detection properties are reproducible by tightly controlling their growth parameters. For the homo-epitaxial ones, diamond is used as a seed for the CVD growth. Diamond nano-crystals are used as substrate for the pCVD (poly-crystal CVD). The resulting diamond bulk contains grain-boundaries corresponding to the junction of crystal growth from different seeds. These structural defects act as charge trapping centers for the free charge carriers. However, the main asset of pCVD diamonds is that they can be grown to large areas of several cm^2 [8]. Besides, sCVD diamond are high quality single-crystal diamonds. The substrate of choice is usually a surface-treated HPHT (High Pressure High Temperature) diamond with a <100> orientation. Unfortunately, the area of these diamonds is restricted up to now to less than 1 cm^2. Last, hetero-epitaxial diamonds are grown using CVD on a substrate with a diamond-like crystal structure, for example iridium (hereafter named as Diamond on Iridium, DOI). They are very promising diamonds with qualities close to the single crystal ones. Moreover, they can be grown up to more than 1 cm^2 area [9], [10].

Compared to other semiconductor detectors, such as silicon ones, detectors based on CVD diamond exhibit several advantages [11], [12], [13], [14]. Their radiation hardness has already been demonstrated. A high resistivity (>10^{13} Ω m) coupled to a large electronic gap (5.48 eV) results in a lower noise level and an almost negligible leakage current even at room temperature. Despite the fact that the energy required to produce electron-hole pairs is 3.6 times larger than in silicon, the signal to noise ratio is higher for diamond. The high charge carrier mobility leads to a very fast detector response allowing excellent time resolution (few tens of picoseconds) and high count rate capability, even for polycrystalline detectors, for which the charge collection efficiency is less than 100%.

Hence, diamond applications are more and more considered in various physics fields. Diamond detectors are commonly used as X-ray synchrotron radiation monitors but also as UV and neutron sensors [15]. In high-energy physics, diamond detectors are used for beam monitoring [16]. In medical physics applications, they are used as dosimeters for radiotherapy [17].

In the present study, we used sCVD and pCVD diamonds from Element6 [8], and heteroepitaxial DOI diamonds from Audiatec [9]. The tested samples were ranging from 300 µm up to 500 µm in thickness, and from 5×5 mm^2 to 2×2 cm^2 area.

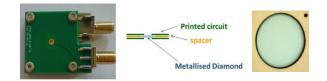### B. Detector processing and pulse signal readout

Fig. 2 The diamond sensor with a disk shaped metallization housed in its socket.

Up to 2016, an aluminum disk shaped metallization was locally performed by using the DMW (Distributed Microwave Plasmas), a technology developed by LPSC [18]. The crystal surface preparation and metal deposition were thus performed by a sequential plasma process consisting in two steps of reactive plasma cleaning followed by plasma-assisted sputtering.

The sensor contact for the disk-shaped metallization consists of a 50 nm thick aluminum layer deposited on both sides. Diamonds are mounted on sample holders with 50 Ω adapted impedance and SMA connectors, enabling reversible bias and signal readout from both sides of the diamond as illustrated by Fig. 2. Several preamplifiers were tested: the CIVIDEC C2 low-noise broadband RF amplifier (2 GHz, 40 dB from CIVIDEC Instrumentation company [19]) and the DBA III (Diamond Broadband Amplifier [20]) from GSI (a similar 2 GHz design with a gain remotely controlled from 0 dB to 38 dB). These amplifiers are intended for use with fast detectors. They exhibit a 50 Ω input impedance and are able to work with FWHM pulse widths of less than 1 ns.
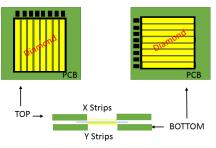

Fig. 3 Scheme of the double-side stripped diamond sensor housed in its dual PCB holder.

In 2017, a double-side strip metallization of the diamond sensors was performed for a position sensitive detector development (one side in X direction and the other in Y

direction, see Fig. 3). The lift-off process was used to create the strips. It consists in creating structures (patterning) using a sacrificial material (e.g., photoresist). This was performed at the NANOFAB laboratory from the Néel Institute. Four steps are needed to perform the strip metallization. At first, S1818 photoresist is deposited on the substrate (10×10 mm^2 diamond). Then the pattern is exposed thanks to an extreme ultraviolet lithography (laser wavelength 405 nm). Development will dissolve exposed pattern. The sample is then metallized with a 100 nm aluminum layer. Residual photoresist is finally lifted away in a solvent with the parts of the undesired metallization. The resulting metallization on the diamond sensor consists of 8 strips of 1 mm width separated by a 100 µm gap and surrounded by a guard ring.

Unlike the case of the disk-shaped metallization, wire bonding ensures the electrical connection between each diamond strip and the PCB. In addition, a set of discrete current amplifiers designed at LPSC (1 GHz, 30 dB) are mounted on the circuit board. The whole set-up is placed inside an electromagnetic shielding box surrounded by SMA connectors to enable bias and signal readout.

If such a detector concept with double-sided stripped diamonds satisfies our requirements (in terms of spatial and timing resolution for a hodoscope development purpose) then we will go one step further with a 2×2 diamond mosaic arrangement. That time, the sensors read out will be performed by a dedicated, multipurpose fast integrated electronics that is currently under development at LPSC.

C. Waveform data acquisition

The pulse shape readout mode was performed with a 500 MHz, 3.2 GS/s digital sampling 'Wavecatcher' [21] system. This system could be configured in a continuous acquisition mode, recording a set of waveforms, and thus enabling large statistics offline analysis.

In addition, a 2 GHz, 20 GS/s analog bandwidth DSO (LeCroy 620Zi) [22] was used. The DSO data acquisition was fully integrated into the ESRF ID21 SPEC software acquisition framework which enabled us to measure the temporal response of the detectors as they were scanned in the beam, thus creating 2D response maps of the detector surfaces.

III. Characterization of CVD Diamonds

A. Leakage current measurement

The quality of the diamond was investigated by measuring the current voltage characteristics. For this purpose, a dedicated test bench was developed. This test setup was also used to highlight possible diamond sparking (electric field breakdown) once the diamonds were metallized. Diamonds exhibit very low leakage current (lower than 10pA in current field operation) as illustrated on Fig. 4, where signals were recorded on a heteroepitaxial DOI.

In our application, diamonds are used as solid state ionization chambers. The charge collection properties of CVD diamond
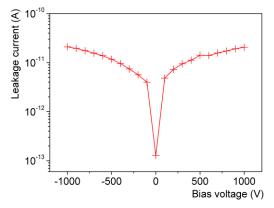
Fig. 4 Measurement on a heteroepitaxial DOI of the leakage current versus the bias voltage.

were investigated with various ionizing particles. We aimed to evaluate the capability of diamond to be used as position sensitive detector.

B. Measurement with α and β particles

Radioactive α sources (^{233}U and ^{241}Am) and β source (^{90}Sr) were setup in dedicated test benches. The mean free path of the α particles (about 12 µm) is much smaller than the diamond thickness. All the current due to the migration of charge carriers comes from a single species (either electrons or holes) traversing the whole detector thickness, depending on the bias polarity. This enabled us to explore the diamond sensitivity to polarization effects and to study the difference in the signal shapes between the growth and substrate sides.

On the contrary, the β set-up enabled us to infer the Charge Collection Distance (CCD) since the electrons emitted by the ^{90}Sr source are traversing the diamond (a trigger on transmitted high-energy electrons is used). As an illustration, a measurement done with a 0.45×0.45 mm$^2 \times$ 518 µm sCVD diamond manufactured by Element 6 is illustrated on Fig. 5. The asymptotic value obtained for the CCD by varying the electric field applied on diamonds electrodes is very close to the diamond thickness. This illustrates the quality of the sCVD diamond.
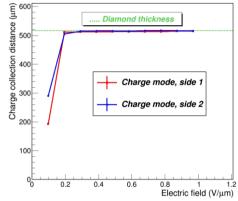
Fig. 5 The charge collection distance measured with the β test bench on a 0.45×0.45 mm$^2 \times$ 518 µm sCVD diamond manufactured by Element 6.
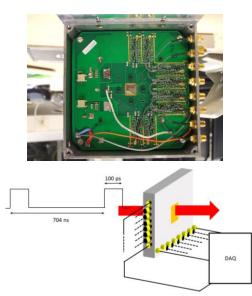
C. Measurements with a pulsed photon beam (8.5 keV).

Fig. 6 ESRF experimental test bench (top : the 1 cm² , double side stripped diamond mounted on the PCB inside an electromagnetic shielding box. 8 discrete in-house preamplifiers are mounted on each side, bottom : the box positioned on the ESRF ID21 beam line).

XBIC (X Beam Induced Current) is of huge interest for our application. In our experiment, a 8.5 keV photon focused micro-beam with a well-defined time structure was used at ESRF. As regards energy deposition in the diamond, 35 % of the beam is absorbed in 300 µm diamond material, which makes the energy deposit almost constant and continuous along the beam path. In the ESRF 4-bunch mode, the ~100 ps duration X-ray pulses, containing a fixed number of photons, adjustable by means of attenuators, with a maximum value of ~1400, mimic the passage of single ionizing particles (maximum energy deposit ~4.1 MeV). Photon bunches are separated by 704 ns intervals, which makes possible individual pulse response measurement, as well as continuous current integration with picoammeters.

The diamond samples were placed inside an electromagnetic shielding box. The box was positioned with micrometric reproducibility at the sample position of the micro-diffraction end station (in air) of the ID21 beamline at ESRF. Fig. 6 illustrates this sample setup for the double side stripped diamond.

D. Measurements with a 95 MeV/u ¹²C ion beam

Finally, to evaluate the diamond performances under carbon ion irradiation, a test with a 95 MeV/u ¹²C ion beam was carried out at the GANIL facility. The energy deposit by such ions in a 300 µm thick diamond is 25 MeV. This experimental set-up enables us to evaluate single carbon ion detection characteristics.

IV. RESULTS

A. Disk-shaped diamond metallization

In the following sections, we report on the charge collection properties of CVD diamonds [23] with disk-shaped metallized sensors (Fig. 2).

1) Pulse shape analysis
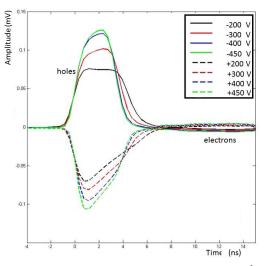

Fig. 7 Signal measurement with an α source on a 0.5×0.5 cm² $\times$ 300 µm DOI detector.

Diamond detectors allow particle identification by pulse-shape analysis. The-pulse shape of the signal collected in diamond material is determined by i) the ionization profile in the diamond sensor, which depends on the particle type and energy, and ii) the transport properties of charge carriers, which depend on the dimensions and properties of the diamond (bias, presence of defects). According to the Shockley-Ramo theoretical description, for very pure crystals such as sCVD diamonds, the shape of the current pulse with incident α particle is rectangular, since it results from drift of a constant amount of charge carriers created close to the surface along the whole crystal thickness. If space charges or trapping defects are present in the diamond bulk, such as for pCVD diamond, the rectangular shape would rather be rhombic. On Fig. 7, the signals recorded on heteroepitaxial diamonds grown on iridium for holes and electrons carriers are plotted by varying the diamond bias voltage using the α test bench. It appears that such diamonds behave as sCVD crystal for the hole carriers and as pCVD for the electron ones. This particular behavior of DOI detector signals was already reported [24].
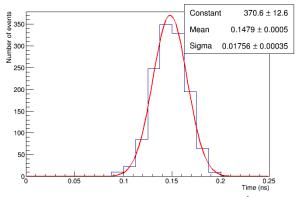
Fig. 8 Time resolution measured between a 0.45×0.45 cm^2 $\times$ 518 µm sCVD diamond and a 0.5×0.5 cm^2 $\times$ 300 µm DOI detector, traversed by a single carbon ion at 95 MeV/u incidence energy.

2) Time resolution measurements

Diamond detectors are expected to be fast responding detectors, as illustrated in Fig. 7, where rise times smaller than 1 ns are observed. Consequently, an offline procedure was established to determine the time resolution of the detectors, based on the waveform analysis. A numerical Constant Fraction Discrimination (CFD) was performed by averaging the background, determining the maximum of the pulses, and interpolating the 50 % rise time value. At the GANIL facility, the dedicated experimental set-up enables us to measure a time resolution between two diamond samples positioned one behind the other. In Fig. 8, a time resolution lower than 18 ps rms was reached using a 0.45×0.45 cm² $\times$ 518 µm single-crystal sample provided by Element 6 coupled to a 0.5×0.5 cm² $\times$ 300 µm DOI provided by Audiatec. The DOI detector was read out with a CIVIDEC preamplifier, and the sCVD with a DBAIII preamplifier, with smaller gain. Thus, this value of timing resolution results from the quadratic sum of both detection device resolutions. Such results with single readout channels are very promising, but, in view of the realization of a multichannel detector prototype, they rely on developments of very fast front-end electronics.

Tests were also carried out at the GANIL facility with a 2×2 cm² $\times$ 500 µm sample coupled to a 1×1 cm² $\times$ 500 µm one. Both diamonds were pCVD ones provided by Element 6. That time, the time resolution was at the level of 90 ps. This result is not in contradiction with the one obtained with the DOI coupled to the sCVD, since the active areas are about one order of magnitude larger here, and the timing resolution depends on the detector capacitance [14].

3) Energy resolution measurements

Energy resolution measurements were performed both at the ESRF and GANIL facilities. At GANIL, with a 95 MeV/u carbon ion beam impacting a 0.5×0.5 cm^2 $\times$ 300 µm polycrystalline diamond, an energy resolution of ~7 % rms was reached (Fig. 9). Using the same diamond sensor, with the 8.5 keV pulsed photon beam at ESRF an energy resolution of ~9% rms was obtained. Such resolutions are good enough to identify unambiguously the passage of a single ion.
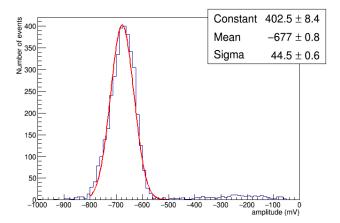

Fig. 9. Energy resolution measured on a 0.5×0.5 cm^2 $\times$ 300 µm poly-crystalline diamond with 95 MeV/u carbon ion beam.
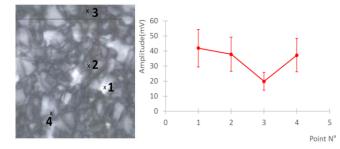
4) Surface mapping

Fig. 10 Amplitude (right) of the signal versus the ESRF-ID21 pencil beam localization from point 1 up to 4 on the current-readout surface map (left) of a 1 mm^2 area of a 1×1 cm^2 $\times$ 500 µm polycrystalline diamond detector.

At the ESRF facility, we have set up a map of the signal response in current integration mode. Fig. 10 shows an example of a polycrystalline detector map (1×1 cm^2 $\times$ 500 µm pCVD detector from Element 6) on a 1 mm^2 area. The grey scale corresponds to the charge collection efficiency measured by an electrometer. Clearly, the response of the detector reflects the spatial distribution of grain boundaries in the polycrystalline material.

In addition, Fig. 10 shows the diamond response versus the photon pencil beam localization for the same pCVD diamond detector. With such a sample, a difference of a factor two is observed between the clearest point and the darkest one. It has been checked that such an amplitude variation will introduce an acceptable time walk in time measurement. This result could be seen as in contradiction with the result of the previous section, where a resolution of 9 % was obtained with a similar pCVD. Nevertheless, note that the present sample is different (1 cm^2) and that we measured the difference between the two extreme response regions of the surface.

B. Double-side stripped diamond

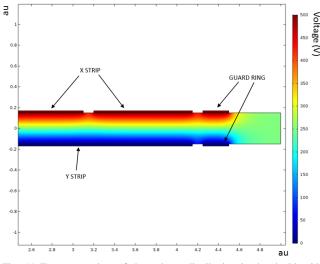*1) Optimization of the strip pitch with a dedicated simulation package*

Fig. 11 Transverse view of the voltage distribution in the double side stripped detector width (COMSOL simulation).

Simulations were carried out using COMSOL Multiphysics [25]. The Fig. 11 illustrates the distribution of the voltage while the X strips on the top side of the diamond are biased at +500 V and the Y ones are ground-biased. At first, it demonstrates the importance of the guard ring which permits all the 8 strips on each side to behave in the same way as far as chagre collection is concerned. Then, the 1mm strip width coupled to the $100\,\mu m$ gap were chosen consequently to these simulations. It was done on one hand to optimize the strip pitch on the 1×1 cm^2 diamond detector surface, and, on the other hand, not to lose too many charges in the gaps.
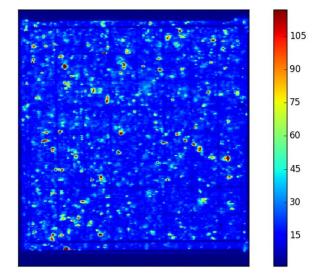

Fig. 12 X-Ray analysis of the surface of a 10×10 mm$^2 \times 300\,\mu m$ double-side stripped pCVD diamond from Element 6.

2) Signal spatial distribution evaluated at the XBIC ID21 beamline of the ESRF facility

We have performed an X-Ray analysis of a double-side stripped diamond surface in a current integration mode (Fig. 12). The non-uniformity of the diamond response quantified by the color scale on the right reflects the defects distribution in the material like on Fig. 10. However, unlike the previous sample, the defect response appear like hot spots (higher current) rather than low response zones.

A zoom of the previous X-Ray analysis (Fig. 12) on a about 2×2 mm^2 area is illustrated by Fig. 13. An ad-hoc adjustment of the colour scale makes visible the inter-strip regions, corresponding to a decrease of the charge collection. This already shows that narrower gaps should be used in order to keep the efficiency constant.

These are preliminary results, a more refined analysis will be performed in a near future, in particular to quantify the cross talk and the reconstructed spatial resolution.
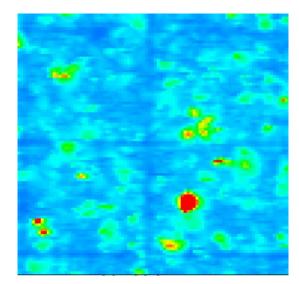

Fig. 13 Zoom of an X-Ray analysis on a about 2×2 mm^2 area of a 10×10 mm$^2 \times 300\,\mu m$ double side stripped pCVD diamond from Element 6.

V. CONCLUSION

Large-area, synthetic pCVD or DOI diamond detectors are foreseen for on-line hadron therapy beam tagging applications. They will be used as a hodoscope which plays a major role for particle identification in time-of-flight gamma camera projects proposed by the CLaRyS collaboration. The radiation hardness, fast response and good signal to noise ratio make diamonds good candidates.

At first, we have carried out tests with disk-shaped metallized diamonds. A time resolution ranging from 20 up to 90 ps rms and an energy resolution ranging from 7 up to 9 % rms were measured when irradiating the whole surface of CVD diamond using various ionizing particles. These results satisfy our requirement despite the obvious non-uniformity of the crystalline structure observed thanks to XBIC analyses. Recently, we have tested double side stripped detectors (8 strips

in X and 8 strips in Y) in a single housing to check signal characteristics.

REFERENCES

[1] H. Paganetti, "Range uncertainties in proton therapy and the role of Monte Carlo simulations," Phys. Med. Biol., vol. 57, no. 11, pp. R99–R117, Jun. 2012.
[2] C.-H. Min, C. H. Kim, M.-Y. Youn, and J.-W. Kim, "Prompt gamma measurements for locating the dose falloff region in the proton therapy," Appl. Phys. Lett., vol. 89, no. 18, pp. 183517–3, Oct. 2006.
[3] E. Testa et al., "Monitoring the Bragg peak location of 73 MeV/u carbon ions by means of prompt γ-ray measurements," Appl. Phys. Lett., vol. 93, no. 9, p. 93506, 2008.
[4] J. Krimmer et al., "Collimated prompt gamma TOF measurements with multi-slit multi-detector configurations," J. Instrum., vol. 10, no. 1, pp. P01011–P01011, Jan. 2015.
[5] J. Krimmer et al., "Development of a Compton camera for medical applications based on silicon strip and scintillation detectors," Nucl. Instrum. Methods Phys. Res. Sect. Accel. Spectrometers Detect. Assoc. Equip, Elsevier, 787, pp 98-101,2015 <doi:10.1016/j.nima.2014.11.042>.
[6] J. Krimmer et al., "Real-Time Online Monitoring of the Ion Range by Means of Prompt Secondary Radiations", published in 3rd International Conference On Advancements In Nuclear Instrumentation Measurement Methods And Their Applications (ANIMMA 2013), Marseille: France 2013.
[7] S. Deng et al.,"Very fast front end ASIC associated with multi-anode PMTs for a scintillating-fibre beam hodoscope", Journal of Instrumentation 8 (2013)C01047. DOI:10.1088/1748-0221/8/01/C01047.
[8] http://e6cvd.com/
[9] http://www.audiatec.de/
[10] M. Schreck et al., "Large-area high-quality single crystal diamond", MRS Bulletin, vol.39, n°6, pp. 504-510, 2014.
[11] P. Bergonzo et al., "CVD diamond for radiation detection devices", Diamond and Related Materials 10 (2001). 631-638.
[12] E. Berdermann and M. Ciobanu, "CVD-Diamond Detectors for Experiments with Hadrons, Nuclei, and Atoms", *CVD Diamond for Electronic Devices and Sensors* Ed. R. S. Sussmann, 2009 John Wiley & Sons.
[13] M. Ciobanu et al., "In-Beam Diamond Start Detectors" IEEE Trans. Nucl. Sci.58, No. 4 (2011).
[14] F Schirru et al "Development of large area polycrystalline diamond detectors for fast timing application of high-energy heavy-ion beams" JINST No 7 (2012) P05005 doi:10.1088/1748-0221/7/05/P05005.
[15] C. Weiss et al., n-TOF collaboration, "A new CVD diamond mosaic-detector ofr (n,α) cross-section measurements at the n-TOF experiment at CERN", proceedings, 13th Vienna Conference on Instrumentation (VCI 2013), Vienna, Austria, February 11-15, 2013, Nucl. Instrum.Meth A732 pp 190-194, 2013.
[16] E. Griesmayer and B. Dehning, "Diamonds for beam instrumentation", in Proceedings of the 2nd International Conference on Technology and Instrumentation in Particle Physics (TIPP 2011), Chicago U.S.A. (2011) [Phys. Procedia 37 p 1997, 2012].
[17] http://www.ptw.de/2968.html
[18] A. Lacoste et al., "Multi-dipolar plasmas for uniform processphysics", design and performance, SCi. Technol., 11 pp 407-412, 2002..
[19] https://cividec.at/_C2_Broadband_Amplifier,_2_GHz,_40_dB.html
[20] P. Moritz, E. Berdermann, K. Blasche, H. Stelzer, B. Voss, "Broadband electronics for CVD-diamond detectors", Diamond and Related Materials 10 pp 1765-1769, 2001.
[21] D.Breton, E. Delagne, J. Maalmi, "Picosecond time measurement using ultra-fast analog memories", proceedings TWEPP2009, Topical Workshop on Electronics for Particle Physics. Paris 21-25 September 2009.
[22] http://teledynelecroy.com/oscilloscope/
[23] M-L Gallin-Martel et al, "Large Area Polycrystalline Diamond Detectors for Online Hadron Therapy Beam Tagging Applications", IEEE Nuclear Science Symposium & Medical Imaging Conference (2016 IEEE NSS/MIC), Oct 2016, Strasbourg, France. in press, Proceedings of the IEEE NSS MIC 2016.
[24] M. Kis et al.,"TCT characterization of new generation of DoI samples", 4th ADAMAS workshop (2014), Dec. 2014, GSI, Darmstadt.
[25] https://www.comsol.com/release/5.3